

## INFLUENCE OF PREHEATING AND OXYGEN CONTENT ON SELECTIVE LASER MELTING OF Ti6Al4V

### ABSTRACT

Selective Laser Melting of Ti6Al4V has already transitioned to commercial exploitation, but is still coping with two major limitations that restrict a more widespread use. Residual stresses can cause a premature build failure by inducing cracks in bigger parts, and deformations of fine features during the build and of the whole part after removal from the build platform. On the other hand, the ductility of the martensitic  $\alpha'$  microstructure is relatively low. Preheating of the build platform may provide a solution for both problems. It reduces thermal gradients and thus limits the development of residual stresses, but also causes a transformation of the  $\alpha'$  microstructure to a more ductile mixture of  $\alpha+\beta$ . In this research, preheating of the base plate up to 400°C shows that residual stresses are reduced by 50%, and a transformation of the microstructure to a  $\alpha+\alpha'+\beta$  mixture. However, pickup of interstitial elements at elevated temperatures during the process leads to an embrittlement, reducing the ductility. Careful control of the atmospheric parameters may eliminate this issue, paving the way for build platform preheating to solve the current problems with SLM of Ti6Al4V.

## 1. INTRODUCTION

In Selective Laser Melting (SLM) a high power laser locally melts successive layers of powder to produce complex shape 3D metal parts. The highly localized heat input leads to fast melting and solidification, resulting in a unique microstructure. SLM possesses several advantages over other production techniques, such as a high material use efficiency, a high level of flexibility and near net shape production of geometrically complex structural parts. The disadvantages are mainly caused by the rapid solidification. Steep thermal gradients in both space and time cause large residual stresses and can also induce deformation or even cracking of the parts. The process details and applications have been widely reviewed elsewhere. For example, the reader is referred to Ref. [1] for more details.

A popular material in aerospace and the medical industry, Ti6Al4V was one of the first materials to be successfully processed by Additive Manufacturing (AM) [1]. Numerous studies have characterized the microstructure for the two powder bed fusion processes, SLM [2-6] and Electron Beam Melting (EBM) [7-9]. It has been established that during both SLM and EBM, partial remelting of previously deposited layers lead to vertical columnar  $\beta$  grains that are, on average, as wide as the hatch spacing and up to several millimeters long due to epitaxial growth. In SLM, the rapid solidification causes the  $\beta$  phase to transform to the acicular martensitic  $\alpha'$  phase. By contrast, during EBM, the temperature of the powder bed is raised to temperatures above 700°C. This way, the powder is presintered, after which the electron beam fully melts the selected vectors. If the powder was not presintered, excessive charging of the powder would cause it to be blown away by the passing electron beam. Because of the high temperature, cooling rates are much lower than in SLM and a lamellar  $\alpha+\beta$  microstructure is generated, while there are almost no residual stresses. These factors combined generally lead to a higher ductility of EBM parts. There is no need for further heat treatments, bar a HIP treatment to eliminate trace porosity. The disadvantage of the high ambient temperature is a high surface roughness and a sintered powder cake from which the parts need to be extracted.

Large residual stresses and a fine  $\alpha'$  martensite lead to a high yield stress (1000-1200MPa) and ultimate tensile strength (1100-1300MPa), but a relatively low ductility (4-8%). Previous research to increase to ductility of SLM produced Ti6Al4V mostly focused on optimized post process heat treatments [3,6,10,11] and also on HIP treatments [3,12]. These heat treatments transformed the acicular  $\alpha'$  martensite to a mix of lamellar  $\alpha$  with interlamellar  $\beta$ , through which the ductility could be increased to above 13% while keeping the strength above acceptable levels. The optimal heat treatment temperature range lies between 850°C and 950°C. These temperatures are high enough to fully transform the martensite and allow reasonable coarsening of the  $\alpha$  lamellae. The columnar prior  $\beta$  grains remain the same size, limiting the  $\alpha$  colony size. These temperatures are low enough to stay below the  $\beta$  transus at 1000°C, above which excessive coarsening of the  $\beta$  grains takes place, resulting in a softer material.

Recently, Xu *et al* [13] were able to induce decomposition of the martensite to a fine lamellar  $\alpha+\beta$  during the SLM process. By varying the layer thickness but also by offsetting the focal point of the laser with the powder bed and using 200°C base plate preheating, they were able to maintain the heat affected zone above a critical temperature for a long enough time to decompose the martensite. This resulted in an increased ductility around 13% without any loss in strength. Meanwhile, Simonelli *et al* [14] independently produced Ti6Al4V samples in which the microstructure varied strongly over the 5mm height. At the bottom near the support structure, the microstructure consists of lamellar and equiaxed  $\alpha+\beta$ , transitioning to the familiar acicular  $\alpha'$  martensite at the top. This was achieved by using a base plate preheating of 200°C, but also by using a low hatch spacing of 30  $\mu\text{m}$  and an extremely low scan speed of 58 mm/s, in order to maximize the interaction time between the material and the laser.

In this research, only base plate preheating is used, but up to 400°C, a preheating temperature not often achieved during SLM. By lowering the thermal gradients, preheating

not only allows decomposition of the martensite, but will also lower residual stresses. However, there will be associated problems such as increased oxygen pickup, which will be highlighted in this paper.

## 2. MATERIALS & METHODS

Plasma atomized Ti6Al4V-ELI (Grade 23) powder with a particle size ranging from 5 to 50  $\mu\text{m}$  and a  $d_{50}$  of 34  $\mu\text{m}$  was used. The jobs were built chronologically with increasing preheating temperature, and the powder was recycled each time for use in the next job.  $10 \times 10 \times 10$  (XxYxZ)mm<sup>3</sup> cubic samples were built for density and microstructure analysis for all parameter sets listed in Table 1.  $20 \times 20 \times 20$  mm<sup>3</sup> cubic samples for stress analysis and  $3 \times 90 \times 15$  mm<sup>3</sup> samples tensile testing were also built using parameter set 9. Bridge shaped specimens, of which the shape is shown in Fig. 7 below, were produced to further determine the influence of preheating on residual stress. All parts were produced on the in-house developed LM-Q machine of the PMA division of the department of mechanical engineering, KU Leuven [15]. Using a continuous Yb:YAG fiber laser, each layer was scanned using a zigzag scanning strategy with a 90° rotation between layers. The density was measured using the Archimedes method.

For microstructural examination, samples were ground using a 1200 grit SiC grinding paper, polished using a SiO<sub>2</sub>-H<sub>2</sub>O<sub>2</sub> suspension and etched with a solution of 50 ml H<sub>2</sub>O, 25 ml HNO<sub>3</sub> and 5 ml HF for 5 to 10 seconds. An Axioskop 40 Pol/40 A Pol microscope was used to examine the microstructure with relatively small magnifications, while a FEI Nova nanoSEM allowed high magnification images. A Siemens D500 diffractometer with Cu radiation was used to determine diffraction spectra based on polished cross sections parallel to the building direction, and residual stress on as-built top surfaces. For the residual stress measurements, the {21-33} peak of the  $\alpha/\alpha'$  phase was used, located around  $142^\circ 2\theta$  for SLM produced Ti6Al4V. The X-ray elastic constants used are  $S_1 = -2.8635 \text{ TPa}^{-1}$  and  $S_2/2 = 1,1694 \text{ TPa}^{-1}$ . These values were calculated with the Voight-Reuss-Hill approximation using the single crystal elastic constants for pure Ti available from Kocks [16].

Oxygen content was determined by Evans Analytical Group using Interstitial Oxygen Analysis (IGA). The Vickers microhardness tests were performed, for 10 seconds each, on a Leitz-Durimet tester using a weight of 500 g. Values in the text are an average of 10 measurements per specimen. Four horizontal tensile specimens per preheating temperature were tested according to ASTM E 8M at a strain rate of 1 mm/min using an INSTRON 4505 machine. Yield stress and Young's modulus were determined according to ASTM E111. The loading direction was perpendicular to the building direction during SLM.

Table 1: Used parameter sets. h = hatch spacing, t = layer thickness, v = scan speed, P = laser power.

h = 70 $\mu\text{m}$	t = 30 $\mu\text{m}$	P [W]		
		50	150	250
	400	1	2	3
v [mm/s]	1000	4	5	6
	1600	7	8	9

## 3. RESULTS & DISCUSSION

The nine different parameter sets were chosen over a wide interval of scan speed and laser power to cover the entire field of parameter sets known to produce good results at the KU Leuven. However, not all parameters sets shown in Table 1 lead to a high density. Looking at Fig. 1, three different density zones stand out. The first zone with the lowest density occurs for the moderate and high speed, 50 W parameter sets. For these sets, the energy input is too low and the melt pool too small to provide sufficient overlap between adjacent scan tracks and between subsequent layers.

In the second zone, with densities between 96% and 99%, the energy input is too high because of the low scan speed (400 mm/s). There will be more vaporization of the material, which will lead to small spherical pores. Moreover, the melting regime could transition to a keyhole mode, creating a deep and narrow melt pool that can collapse on itself and trap gas [17]. Finally, using moderate to high scan speeds and moderate to high laser powers creates a stable melt pool that leads to densities higher than 99.5%. These three zones are present for all preheating temperatures. Moreover, the densities do not change significantly by changing the preheating temperature. Theoretically, by increasing the surrounding temperature, less energy input would be needed from the laser to melt the powder and create a suitable melt pool. This could increase the density of parameter sets in the first zone, where energy input is not high enough. It could also push the energy input of some parameter sets above what is strictly needed and lead to more unstable melt pools, lowering the density. This would affect parts in the second and third region. In this study, the non-influence of the preheating temperature does not mean that it does not have the predicted effect. For example preheating temperature had a large effect on density on a nickel super alloy and a tool steel (unpublished results). All further results will be based on specimens produced with parameter set 9 (1600 mm/s and 250 W).

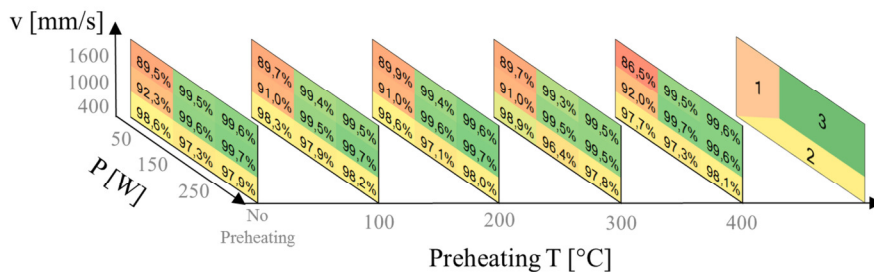


**Fig. 1: Density of the 10x10x10 mm<sup>3</sup> test cubes for the various parameter combinations.**

Shown in Fig. 2, the XRD spectra indicate that the martensitic microstructure is still present when a preheating temperature of 200°C is used. The strongest  $\beta$  peak that does not overlap with  $\alpha/\alpha'$  peaks is located at a diffraction angle around  $57^\circ 2\theta$ , and belongs to the  $\{200\}$  crystal planes. At 300°C preheating, the  $\beta_{\{200\}}$  peak is starting to become apparent, but would be invisible in the background noise without long measuring times, and without magnification it would not be visible in comparison to the  $\alpha/\alpha'$  peaks. Even though the  $\beta$  fraction is still very small, its presence proves that martensite decomposition is already taking place using a preheating of 300°C. Either the thermal gradients are low enough to result in an incomplete transformation of the material to martensite, or that the HAZ remains above a critical temperature long enough to allow decomposition of the martensite. At 400°C, the  $\beta_{\{200\}}$  peak is even more present. Concerning the  $\alpha/\alpha'$  peaks, it is impossible to distinguish if they belong to the martensitic  $\alpha'$  phase or the  $\alpha$  phase, since both crystal structures are near identical. However, it is safe to assume that if there are no  $\beta$  peaks, the material consists fully of  $\alpha'$  martensite.

Even though the diffraction spectra indicate a significant change in phase composition, there is no apparent difference in the macrostructure of samples produced without preheating (NP) and those produced with 400°C preheating, shown in Fig. 3. Both macrostructures show long, columnar prior  $\beta$  grains, in which a fine plate like structure is visible. A horizontal banded structure is visible in both microstructures, but is much more pronounced using 400°C preheating. The structure is repeated roughly every 120  $\mu\text{m}$ , or every 4 layers. Given that the scan strategy used a  $90^\circ$  rotation between layers, this means that the band structure repeats for every full rotation of the scan strategy. The phenomena which cause these bands are part of further investigation.

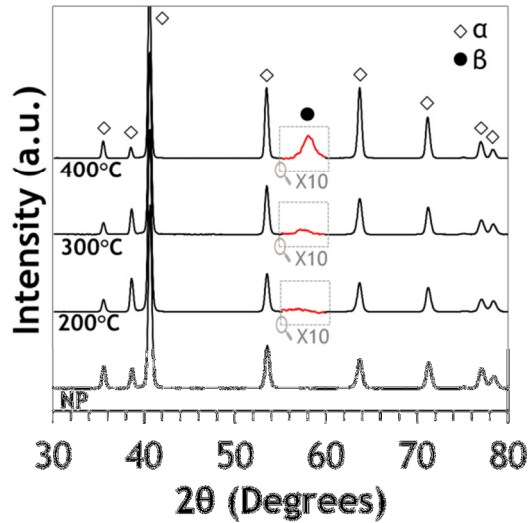


Fig. 2: X-ray Diffraction spectra prove that the microstructure is transformed from  $\alpha'$  without preheating to a  $\beta$  containing microstructure by using a preheating of 300°C or higher.

In Fig. 4, the difference between both seemingly similar plate like structures is revealed. Without preheating, acicular  $\alpha'$  martensite is visible, of which the individual plate edges are straight and jagged. Moreover, many plates seem to be riddled with twin structures. These twins accommodate the dimensional changes that accompany the  $\beta$  to  $\alpha'$  transformation. Using 400°C preheating, the microstructure is not only coarser, but it can no longer be called acicular. This lamellar structure shows fine  $\alpha/\alpha'$  plates, in between which a thin layer of  $\beta$  phase exists. The equilibrium  $\beta$  phase fraction in Ti6Al4V is around 10%. The  $\beta$  fraction in the current microstructure is significantly lower than 10%. This indicates that some  $\alpha'$  must still be present. The mechanism behind these transformed microstructures is the decomposition of the martensite in the heat affected zone (HAZ) in lower layers, when a new layer is added. According to Xu *et al* [13], this mechanism takes place for regions in the HAZ that experience temperatures above 400°C, which is the maximum preheating temperature used in this study. This transformed microstructure should lead to a more ductile and softer material. The difference of this study with that of Xu *et al* [13] and Simonelli *et al* [14] is that both studies used slow parameter sets, increasing the interaction time of the material with the laser. In this study, a fast 1600 mm/s scan speed (compared to 58 mm/s for Simonelli *et al* [14]) is used, making this method more economically viable.

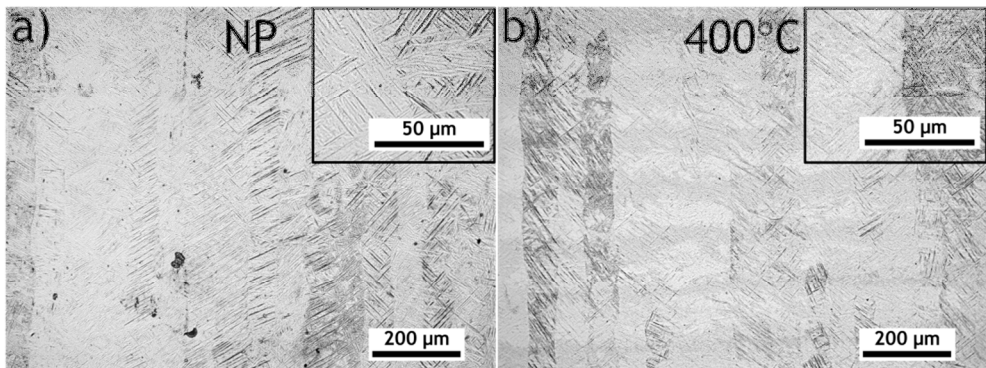


Fig. 3: Columnar prior  $\beta$  grain macrostructure in both the material built without preheating (a) and using 400°C preheating (b). Some horizontal banding is present in b).

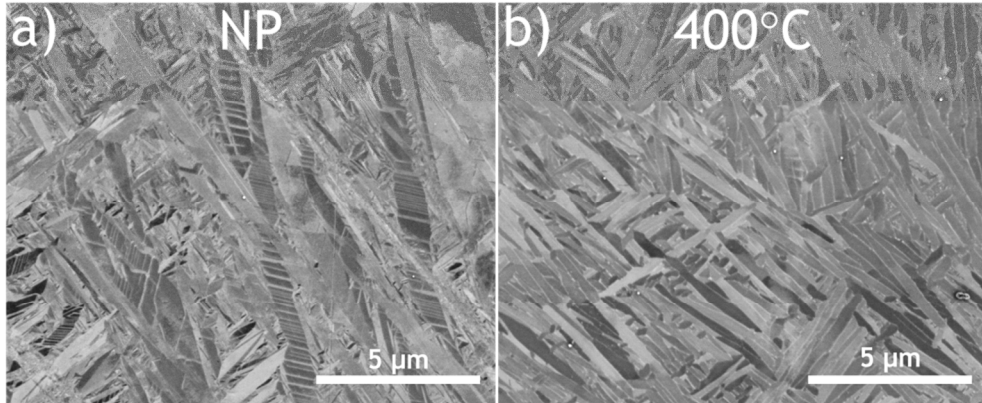


Fig. 4: a) Martensitic microstructure without preheating shows straight, jagged lines delineating the martensite plates, some of which contain a multitude of twins. b) While the  $\alpha$  plates have the same size as the martensite, the edges are rounded and sometimes house a thin layer of  $\beta$  phase.

While the shift to a lamellar  $\alpha+\alpha'+\beta$  microstructure is expected to soften the material, the hardness, shown in Fig. 5, actually increases with increasing preheating temperature. The hardness at the top of the sample rises from  $414 \pm 4$  to  $459 \pm 6$  HV<sub>0,5;10s</sub>, and there is a difference between the top and bottom of the part that increases with increasing preheating temperature. The microstructure has changed, but so has the composition. A drastic increase of oxygen and nitrogen concentration, see Table 2, hardened the material. The powder composition is below the specifications for Grade 23, Extra Low Interstitial Ti6Al4V, even after processing at 400°C and a visible discoloration from metallic grey to a grey-brown color, which apparently only affects the outer layer of the particles. Meanwhile, the parts do pick up a significant amount of oxygen and nitrogen, even without preheating, and can no longer be classified as Grade 23, but as Grade 5 Ti6Al4V. Even though the builds occur in an argon atmosphere (generated from liquid argon), trace oxygen and nitrogen are easily picked up by the hot melt pool. With increasing preheating temperature, it is thought that the temperature of the melt pool increases, thereby also increasing the oxygen and nitrogen concentration in the final parts.

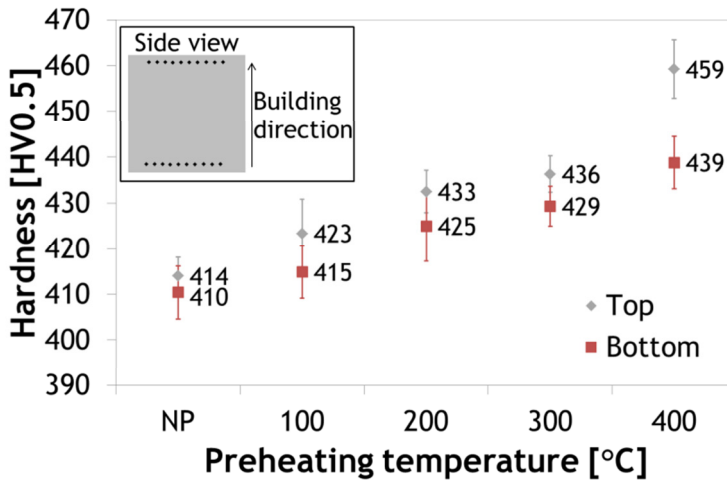


Fig. 5: Rather than the expected softening of the material, the hardness increased with increasing preheating temperature. The difference between the top and bottom of the part also becomes significant at 400°C preheating.

**Table 2: Oxygen and nitrogen concentration of the powder and of parts produced at different preheating temperatures.**

	O [ppm]	N [ppm]
Ti6Al4V Grade 5	Max. 2000	Max. 500
Powder	1170 ± 180	92 ± 26
Powder 400 °C	1180 ± 130	139 ± 63
NP	1660 ± 35	384 ± 20
200 °C	1940 ± 53	594 ± 65
400 °C	2380 ± 42	552 ± 36

The difference between the top and bottom part is due to the fact that the material at the bottom has been influenced more by the heat coming from the many layers on top of it, while the layers at the top did not receive this thermal history of repeating reheating, at least not as much. The bottom has thus had more opportunity to transform to the softer, lamellar structure. The top, consists of harder acicular martensite. Using a 60 µm layer thickness (double that used in this study), Xu *et al* [13] deposited at least eight layers without occurrence of martensite decomposition. This translates to a fully martensitic zone near the top of roughly 500 µm deep in which the hardness measurements were performed. The effect of the oxygen and nitrogen is also visible on the tensile properties, which are summarized in Table 3. The material yields around 1100 MPa for preheating temperatures up to 100 °C. For higher preheating temperatures, the yield stress rises to above 1200 MPa using 400 °C preheating. Another noticeable effect is that the material becomes stiffer, but unfortunately, also less ductile. In general, the effect of interstitial nitrogen is more important than that of oxygen in HCP Ti [18]. Using a state of the art transmission electron microscopy with a 50 pm resolution, in-situ mechanical tests and first principles calculations, Yu *et al* [19] found that the core structure of edge dislocations in HCP pure Ti was not significantly affected by oxygen content, but that of screw dislocations was. The strong pinning effect of the oxygen interstitials on screw dislocations leads to a significant increase in yield strength. While their analysis focused on oxygen, it is also valid for other interstitial solutes such as nitrogen and carbon. For low N concentrations (<1000ppm) in particular, a small increase in concentration leads to a dramatic reduction in ductility [20].

**Table 3: Mechanical properties of parts produced at different preheating temperatures.**

	E [GPa]	$\sigma_y$ [MPa]	UTS [MPa]	$\epsilon_f$ [%]
NP	113 ± 2	1088 ± 14	1221 ± 15	6.9 ± 1.9
100 °C	113 ± 1	1092 ± 22	1234 ± 26	6.4 ± 1.2
200 °C	115 ± 1	1135 ± 11	1234 ± 7	3.7 ± 1.2
300 °C	118 ± 1	1147 ± 7	1230 ± 7	4.5 ± 0.8
400 °C	118 ± 1	1215 ± 13	1280 ± 11	3.9 ± 1.4

A beneficial effect of lowering the thermal gradients was the 50% decrease in residual stress. Illustrated in Fig. 6, the maximum residual stress in the top surface of a 20x20x20 mm<sup>3</sup> cube, measured by XRD, decreases from 630 MPa without preheating to 310 MPa with 400 °C preheating. The top layer has never been part of the HAZ of layers deposited on top of it, and thus has not received any short in-situ heat treatment. As mentioned above, the hardness measurements indicate that the top still consists of  $\alpha'$  martensite. The decrease in stress in the top layers must thus be attributed to the lower overall thermal gradients. By contrast, the bulk of the sample has undergone repeated thermal cycling, and each thermal cycle may induce a small stress relieving effect. This is visible in Fig. 7, where the deformation of bridge-shaped structures, shown in the insert in Fig. 7, are shown. The curvature of the bridges produced without preheating is double that of bridges produced with 400 °C preheating. A Coord3 CMM machine with a 3mm stylus was used to measure the deformations of the bridge shaped specimens. Four measurement points were taken across the width of the sample, and 24 points along the length. The values reported are an average of the measurement points along the width, again averaged for the two bridges built per preheating temperature. While there is no apparent difference for the samples produced without preheating, 100 °C, and 200 °C preheating, there is a significant drop in curvature for the 300 °C and 400 °C specimens. The large decrease in curvature between

using 300°C and 400°C preheating furthermore suggests that a moderate further increase in preheating temperature may lead to a large beneficial decrease of residual stress.

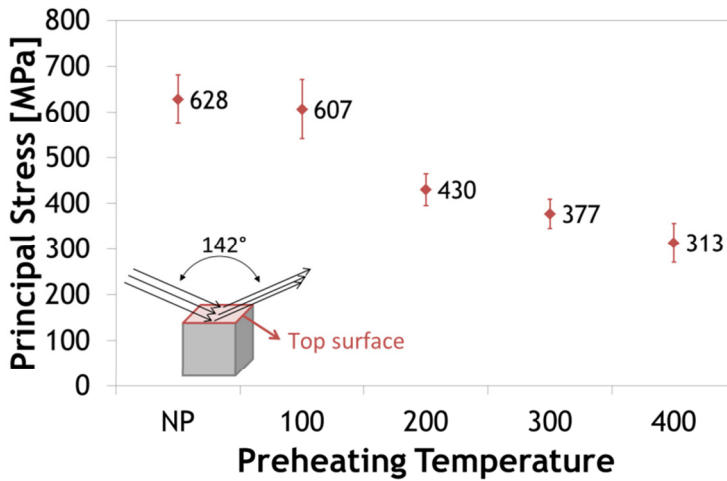


Fig. 6: Residual stress in the top surface of a bigger cube, measured by XRD, shows a 50% drop when preheating at 400°C is employed.

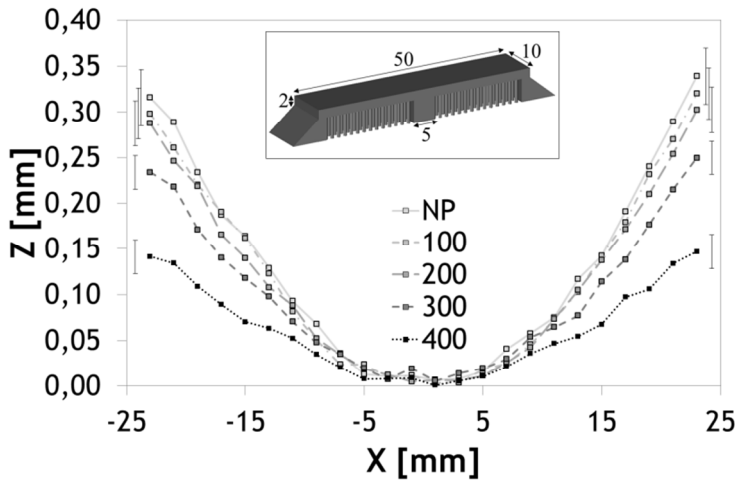


Fig. 7: Deflection of the overhang structure after removal from the base plate is reduced by 50% by using preheating.

In order to determine the residual stresses that were relaxed by the measured deformation of the bridges, the deformation was applied to a 2D ABAQUS FE model of an original, undeformed and stress free bridge structure. Because the deformations are small, the resulting stresses can be assumed to be the same, but inverted, as those that would have been obtained using an FE model of the deformed structure and returning it to the original shape. The stresses are inverted, since in the current situation the stresses are supposed to be the cause of the deformation, and not the other way around. The model consisted of standard linear elements, type CPS4R. In total, nine square elements span the 2 mm height of the thin section, of which a part is shown in Fig. 8.

To avoid stress discontinuities or unrealistic peaks due to measurement uncertainties, a smooth parabolic curve was fitted through the measured deformations, resulting in good

fits with a minimum R<sup>2</sup>-value for all curves of 0.9854 (in the case of the 400°C preheating curve). This curve was then evaluated at the locations of the nodes in the FE model and applied as a boundary condition. The inverted resulting stress profile is shown in Fig. 8 for the deformation without preheating and with 400°C preheating.

The results can be checked by calculating the stress using the Euler-Bernoulli beam theory. From the parabolic fit mentioned above, the curvature was calculated using Equation 1. Then, the stress profile over the height of a beam, bent with a radius  $\rho$  ( $= 1/\kappa$ ), can be calculated using Equation 2. Again inverting the sign of the stresses creates the curves in Fig. 8. There is a perfect overlap between the results obtained by ABAQUS and those calculated using the beam theory, apart from edge effects at the top and bottom of the FE model. Keep in mind that the measured deformations are the result of the elastic relaxation of only an unknown part of the residual stresses. The actual residual stress state is complex and is may not even be linear.

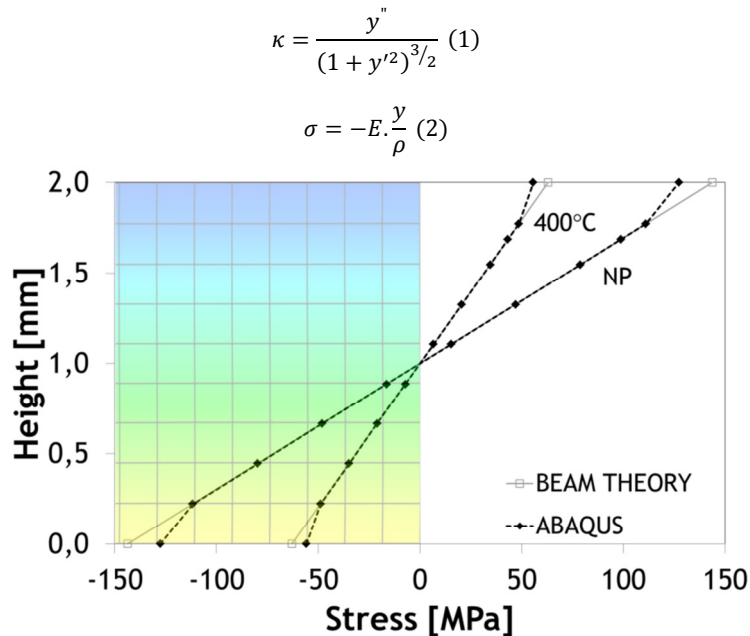


Fig. 8: The stress profile in the overhang structure, necessary to create the measured deformation. The mesh of the FE model is shown as well.

#### 4. CONCLUSION

The influence of preheating on Selective Laser Melting of Ti6Al4V was studied for nine different parameter sets. There was no discernable influence of the preheating on density, but the microstructure changed from acicular  $\alpha'$  martensite to lamellar  $\alpha+\alpha'+\beta$  at a preheating of 400°C due to partial decomposition of the martensite in the heat affected zone. The residual stresses are reduced by 50%, but excessive pick-up of oxygen and nitrogen during the process caused the ductility to drop from around 7% in the as built state to 4% using 400°C preheating. However, the results show that base plate preheating is a viable method to produce more ductile Ti6Al4V while reducing residual stress, if precautions are taken to avoid oxygen and nitrogen pickup.

#### REFERENCES

- [1] J. P. Kruth et al 2007. Consolidation phenomena in laser and powder-bed based layered manufacturing, *Cirp Ann. Technol.*, 56(2), pp 730-759.

- [2] L. Thijs et al 2010, A study of the micro structural evolution during selective laser melting of Ti-6Al-4V, *Acta Mater.*, 58(9), pp. 3303-3312.
- [3] L. Facchini et al 2010, Ductility of a Ti-6Al-4V alloy produced by selective laser melting of prealloyed powders, *Rapid Prototyp. J.*, 16(6), pp. 450-459.
- [4] M. Koike et al 2011, Evaluation of Titanium Alloys Fabricated Using Rapid Prototyping Technologies-Electron Beam Melting and Laser Beam Melting, *Materials (Basel)*, 4(10), pp. 1776-1792.
- [5] I. Yadroitsev, P. Krakhmalev, and I. Yadroitsava 2014, Selective laser melting of Ti6Al4V alloy for biomedical applications: Temperature monitoring and microstructural evolution, *J. Alloys Compd.*, 583(0), pp. 404-409.
- [6] T. Vilaro, C. Colin, and J. D. Bartout 2011, As-Fabricated and Heat-Treated Microstructures of the Ti-6Al-4V Alloy Processed by Selective Laser Melting, *Metall. Mater. Trans. A Phys. Metall. Mater. Sci.*, 42A(10), pp. 3190-3199.
- [7] L. E. Murr et al 2009, Microstructures and mechanical properties of electron beam-rapid manufactured Ti-6Al-4V biomedical prototypes compared to wrought Ti-6Al-4V, *Mater. Charact.*, 60(2), pp. 96-105.
- [8] L. Facchini et al 2009, Microstructure and mechanical properties of Ti-6Al-4V produced by electron beam melting of pre-alloyed powders, *Rapid Prototyp. J.*, 15(3), pp. 171-178.
- [9] N. Hrabe and T. Quinn 2013, Effects of processing on microstructure and mechanical properties of a titanium alloy (Ti-6Al-4V) fabricated using electron beam melting (EBM), Part 2: Energy input, orientation, and location, *Mater. Sci. Eng. A*, 573, pp. 271-277.
- [10] B. Vrancken et al 2012, Heat treatment of Ti6Al4V produced by Selective Laser Melting: Microstructure and mechanical properties, *J. Alloys Compd.*, 541(0), pp. 177-185.
- [11] T. Sercombe et al 2008, Heat treatment of Ti-6Al-7Nb components produced by selective laser melting, *Rapid Prototyp. J.*, 14(5), pp. 300-304.
- [12] L. E. Murr et al 2012, Metal Fabrication by Additive Manufacturing Using Laser and Electron Beam Melting Technologies, *J. Mater. Sci. Technol.*, 28(1), pp. 1-14.
- [13] W. Xu et al 2015, Additive manufacturing of strong and ductile Ti-6Al-4V by selective laser melting via in situ martensite decomposition, *Acta Mater.*, 85, pp. 74-84.
- [14] M. Simonelli, Y.Y. Tse and C. Tuck 2014, The formation of  $\alpha+\beta$  microstructure in as-fabricated selective laser melting of Ti-6Al-4V, *J. Mater. Res.*, 29(17), pp. 2028-2035.
- [15] J. Van Vaerenbergh 2008, *Process optimisation in Selective Laser Melting*, PhD Thesis. University of Twente, Twente.
- [16] U. F. Kocks et al 2000, *Texture and Anisotropy: Preferred Orientations in Polycrystals and their Effect on Materials Properties*. Cambridge University Press.
- [17] W. E. King et al 2014, Observation of keyhole-mode laser melting in laser powder-bed fusion additive manufacturing, *J. Mater. Process. Technol.*, 214(12), pp. 2915-2925.
- [18] L.-P. Lefebvre, E. Baril, and L. de Camaret 2013, The effect of oxygen, nitrogen and carbon on the microstructure and compression properties of titanium foams, *J. Mater. Res.*, 28(17), pp. 2453-2460.
- [19] Q. Yu, L et al 2015, Metallurgy. Origin of dramatic oxygen solute strengthening effect in titanium, *Science*, 347(6222), pp. 635-639.
- [20] H. Conrad 1981, Effect of interstitial solutes on the strength and ductility of titanium, *Prog. Mater. Sci.*, 26(2-4), pp. 123-403.